General Model for Thermochemical Ablation into a Vacuum

Timothy K. Risch* and Bernard Laub†
Acurex Corporation, Mountain View, California

A model is presented for the prediction of ablation rates and surface temperatures of laser-hardening materials subjected to high heating rates. The model incorporates translational nonequilibrium gas flow at the surface, sonic outflow constraint at the equilibrium gas state away from the surface, general thermochemistry, and in-depth heat conduction. The effects of surface irreversibilities and sonically limited transfer rates are incorporated into a new code that generates input for modified versions of existing ablation-conduction programs. Comparison of the predictions with experimental data for surface temperature and recession confirms the accuracy of the model for carbon phenolic at irradiances from 0.3 to 5 kW/cm².

Nomenclature

B_i = pre-exponential factor for component i
C_p = heat capacity at constant pressure
C_v = heat capacity at constant volume
e = energy flux
E_{ai} = activation energy for component i
f = molecular distribution function
F = surface view factor
h = enthalpy
$\bar{h}$ = weighted solid enthalpy defined as $(\rho_v H_v - \rho_c H_c)/(\rho_v - \rho_c)$
I_0 = incident irradiance
J = total mass flux
k = thermal conductivity
L = length of Knudsen layer
$\dot{m}$ = mass flow rate
m_i = dimensionless bulk velocity at the e state for species i
M = molecular weight
p = pressure
P = momentum flux
q_{cond} = surface heat loss due to conduction
R = universal gas constant, 8.314 J/mole-K
$\dot{s}$ = surface recession rate
T = absolute temperature
u = bulk velocity at the e state
x = coordinate variable, origin fixed to the receding surface
y = coordinate variable, origin fixed to the material backwall
α = surface absorptivity
α_c = condensation coefficient
α_v = vaporization coefficient
β = backscattering parameter
γ = ratio of specific heats, C_p/C_v
Γ = resin volume fraction
ϵ = surface emissivity
ψ = decomposition exponent
θ = time variable
ξ = molecular gas velocity in the x direction
η = molecular gas velocity in the y direction
ζ = molecular gas velocity in the z direction
λ = mean free path length
ρ = density
σ = Stefan-Boltzman Constant, 5.67×10^{-8} W/m²-K⁴

Subscripts

A = denotes first pyrolyzing component of resin
b = bulk, freestream properties or backscattered flux
B = denotes second pyrolyzing component of resin
c = char gas state
C = denotes reinforcement
e = well-mixed state
g = pyrolysis gas state
i = species i
int = internal energy
r = residual density
s = surface state
sol = solid state at temperature T_s
tot = total energy, translational plus internal
tr = translational energy
v = denoting virgin material state
$\pm$ = bulk solid properties

Introduction

PROPOSED engagement scenarios for continuous-wave space-based laser defense systems require a significant portion of the encounters to occur at high altitudes. To counter such a threat, the application of ablative materials to strategic boosters has been considered as a means of hardening these systems against laser irradiation. High-irradiance laser-target interactions in the upper atmosphere can produce rapid decomposition and ablation of the hardening materials into the low-pressure environment. Accurate predictions of material response under low pressures are needed to assess the vulnerability of present strategic systems and determine the optimum hardening concept for a given threat.

The phenomenon of thermochemical ablation has been studied in great detail.[1,2] This process is now understood to the point where the behavior of many ablative materials can be predicted quite accurately under limited environmental conditions. Previous work has concentrated on understanding ablation under relatively low to moderate ablation rates at or near ambient pressures. Less work has been performed in understanding the process of rapid ablation which occurs with the high heating rates typical of high-energy laser irradiation

Presented as Paper 87-1515 at the AIAA 22nd Thermophysics Conference, Honolulu, HI, June 8-10, 1987; received Jan. 28, 1988; revision received Dec. 13, 1988.

*Staff Engineer, Aerotherm Division, Thermophysics Department. Member AIAA.

†Manager, Aerotherm Division, Thermophysics Department. Member AIAA.

combined with the low-pressure environments expected in the outer atmosphere.

To simulate ablation under radiation heating, the Air Force has funded the development of Aerotherm Prediction Procedure for Laser Effects (APPLE) code.[3] The APPLE code is based on the underlying fundamental principals of physics and chemistry and considers the interactions between surface thermochemistry, fluid dynamics, and subsurface heat conduction in the ablation process. The APPLE code is general and can be applied to many different materials and configurations. This facilitates rapid comparisons of alternative designs with accurate results.

The APPLE code is limited, however, to moderate-rate ablation into atmospheric or near-atmospheric environments. The assumptions on which the APPLE code were derived begin to break down as the pressure of the external environment is lowered, or as the material flux from the surface is increased. One must be knowledgeable in interpreting simulated results from the APPLE code under high-flux or low-pressure conditions. In this work, we have improved upon the APPLE code to accurately treat high-rate ablation into a low-pressure external atmosphere. The improvement to the model is general and retains the fundamental basis and flexibility inherent in the APPLE code. The improved methodology presented here can still be applied to a wide range of proposed hardening materials and design configurations.

Proposed candidate booster hardening materials can be divided into two general classes—charring and noncharring materials. Noncharring materials ablate via reactions which occur only at the material surface. Such materials do not "char" or pyrolyze via in-depth decomposition reactions. Pure graphite and unreinforced silica or carbon are common examples of noncharring materials. More complicated ablative processes are demonstrated by charring or pyrolyzing materials where in-depth decomposition of the material is observed. Polymeric reinforced composites are the most common types of charring materials, since the resin may decompose in locations far removed from the ablating surface. Heat that penetrates into the depth of the material via thermal conduction can cause subsurface reactions to occur, giving rise to substantial variations in the solid properties. Charring or decomposing materials are far more difficult to model than noncharring materials, since the decomposition rate and the ablating gas composition are determined by conditions throughout the material and not just at the ablating surface.

This paper will address the behavior of charring and noncharring materials when exposed to a high-energy laser under low-pressure conditions. A model, capable of simulating the response of generic materials to laser irradiation, will be presented. Specific examples of laser-material interactions will be cited, and the results of some selected calculations will be shown.

The differences between ablation into an atmospheric environment and high-rate ablation into a low-pressure environment are illustrated in Fig. 1. In Fig. 1a, the ablation of a solid under a near-atmospheric pressure is shown. Here, the external flow that may be present forms a smooth boundary layer which travels across the ablating solid. Under these conditions, ablation is characterized by generally low transfer rates, a surface that is in near equilibrium with the adjacent vapor, and a pressure at the ablating surface that is equal to the freestream pressure.

In a low-pressure environment under high-irradiance-level irradiation, the ablation of material will tend to form a jet, rising normally from the surface and separating the external flow. This is illustrated in Fig. 1b. Here, if the transfer rate of the material is high, the conditions at the ablating surface may be quite different from those in the vapor, even very close to the surface. The assumption of surface equilibrium may not be appropriate. Under high ablation rates, the transfer rate can also be limited, since the ablation products leaving the material surface start subsonic, but then accelerate to supersonic conditions. At some point, the flow will become sonic, and the bulk freestream cannot impress itself upon the surface. This sonic limitation will cause the surface pressure to exceed the pressure far out in the bulk. It is these three conditions of 1) surface irreversibilities, 2) sonically limited transfer rates, and 3) a surface pressure not necessarily equal to the freestream pressure that differentiates these two ablation modes.

Previous Work

The fundamental assumption of the model is the existence of a thin region just above the ablating surface designated the "Knudsen Layer." Here, gross changes of temperature, pressure, and vapor-phase composition occur over a length scale comparable to a few mean free paths of molecules. The Knudsen Layer can be considered as a gas dynamic discontinuity, where gas molecules within this zone are not in equilibrium. Physically, molecules that are ejected from the surface, on the average, have a greater momentum and energy than those molecules returning from the bulk. Within the Knudsen Layer, the molecules collide and become equilibated at points away from the ablating surface.

Anisimov[4] was first to suggest that the changes across the Knudsen Layer could be rigorously determined by considering conservation of mass, momentum, and energy across it. He formulated a set of conservation equations around the Knudsen Layer, subject to some basic assumptions, applicable to the vaporization of a monotonic single-component gas from a noncharring material. Recently Knight[5] and Baker[6] extended this analysis to consider more complex gases and gas mixtures. Knight extended the work of Anisimov to predict the effects of high-rate vaporization of aluminum, which occurs by the transition of solid aluminum into monotonic gaseous aluminum. He also developed a model for the transient flow outside the Knudsen Layer accompanying very short-duration irradiations. Baker modified the conservation equations proposed by Anisimov to determine the steady-state sublimation rate of carbon, which form several different gas phase species upon vaporization. Finally, Risch and Kelly[7] improved on the model of Baker and showed that transient heating effects within the solid phase must be considered if accurate results are to be obtained.

Until now, a general thermochemical model for high-rate ablation has not been developed. Such a model must be

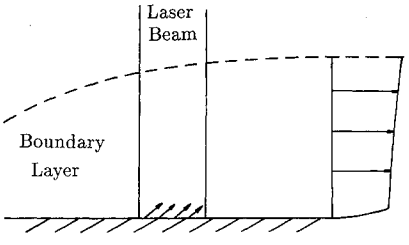

a) Boundary layer type interaction

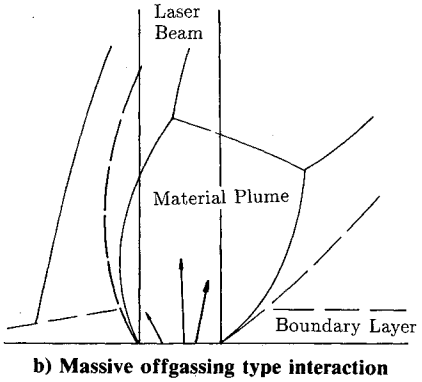

b) Massive offgassing type interaction

Fig. 1 Atmospheric vs vacuum ablation.

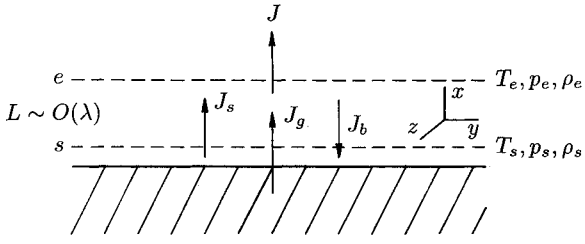

Fig. 2 Property variations at the solid-vapor interphase.

capable of treating materials of arbitrary composition unlike the previous models that are specific only to a few hardening materials. In addition, no work has been performed in treating charring materials that constitute a large class of candidate materials.

Formulation of the Model

Figure 2 illustrates the fluxes and states of the gas in the Knudsen Layer near the interface between the solid and vapor. The two planes, designated by the subscripts s and e, represent the gas-solid interface and an equilibrated state in the gas phase, respectively. The exact position of the e plane is somewhat arbitrary, but it is located away from the surface by a distance L on the order of several molecular mean free paths λ. The s surface, however, is fixed in the gas phase, just outside the solid. In this region, there is a transition from the nonequilibrium properties T_s, p_s, and ρ_s to be the equilibrium gas properties T_e, p_e, and ρ_e at e. The net mass flux of material away from the surface at e denoted by J is equal to the difference between the three components J_s, J_g, and J_b. Flux J_s is due to surface evaporation, and the thermodynamic state of this flux is associated with conditions on the surface. It is assumed that molecules leaving the surface are in equilibrium with solid molecules located just below the adjacent s plane. Flux J_g is due to in-depth generation of pyrolysis gases that are generated from decomposing material far away from the surface. Pyrolysis gases are the result of in-depth thermal decomposition and percolate through charred material to the surface where they pass through the Knudsen Layer. Molecules returning to the surface, flux J_b, are due to the random motion of molecules induced by collisions in the gas away from the material surface. The difference between the thermodynamic states at s and e depends upon the degree of vaporization at the surface. The higher the flux J, the further from equilibrium the surface and vapor become, and the greater the variation of thermodynamic properties across this layer.

Governing Equations

The starting point for the development of the model is the molecular distribution functions for the gas in the Knudsen Layer proposed by Anisimov. These are applicable to any single-component gas with unity condensation and vaporization coefficients (the significance of these will be discussed later). Utilizing the distribution functions and conservation of mass, momentum, and energy, relationships can be constructed to give the change in properties across the thin Knudsen Layer.

For the equilibrium state of the gas at the edge of the Knudsen Layer, or the e state, at the outflow velocity u, a standard Maxwellian distribution is appropriate and is given by the following expression for the molecular distribution function f:

$$f = \rho_e (2\pi RT_e)^{-3/4} \exp\left[-\frac{(\xi - u)^2 + \eta^2 + \zeta^2}{2RT_e/M_e} \right] \qquad (1)$$

The variables ξ, η, and ζ are the molecular velocities in the x, y, and z directions, respectively, where the x direction is taken perpendicular to the ablating surface. The symbol M denotes the molecular weight of the gas-phase species. At the phase interface s, molecules are vaporized from the surface with a positive velocity determined by the equilibrium temperature of the solid. The distribution function is then

$$f_s = \rho_s (2\pi RT_s)^{-3/2} \exp\left[-\frac{\xi^2 + \eta^2 + \zeta^2}{2RT_s/M_s} \right] \qquad \xi > 0 \quad (2)$$

and is limited to only positive velocities (i.e., $\xi > 0$). The molecules that return to the surface are assumed to be scattered from collisions occurring near the equilibrium state e, and only a fraction β of these molecules are assumed to return to the surface. The distribution function for the backscattered molecules is then given by

$$f_b = \beta f, \qquad \xi < 0 \qquad (3)$$

The backscattering coefficient β is an unknown quantity which cannot be specified a priori, but will be determined uniquely by the solution scheme presented later.

Anisimov did not account for pyrolyzing materials in his analysis but, instead, only considered materials that vaporize at the surface. We assume that pyrolysis gas entering the Knudsen layer at the surface is in a state of translational equilibrium and is at a temperature equal to the surface temperature of the solid. Thus, the distribution function for the pyrolysis gas is

$$f_g = \rho_g (2\pi RT_s)^{-3/2} \exp\left[-\frac{(\xi - u_g)^2 + \eta^2 + \zeta^2}{2RT_s/M_g} \right] \qquad (4)$$

At steady state, conservation of mass requires that the elemental mass fluxed into the gas at the s and g state must be equal to the elemental mass fluxes leaving at the e state. Mathematically,

$$J = J_s + J_g - J_b \qquad (5)$$

The fluxes can be obtained from the first moment of the velocity distributions given in Eqs. (2–4). In addition, for a multicomponent gas, the velocity distributions for each species i can be summed to obtain the total mass flux. This is expressed as

$$J = \sum_i \int \xi_i f_i \, dV_i \qquad (6)$$

where

$$dV_i = d\xi_i \, d\eta_i \, d\zeta_i \qquad (7)$$

Carrying out the integration of the distribution fluxes given for J_s and J_b

$$J_s = \sum_i \alpha_{v,i} \rho_{s,i} \sqrt{\frac{RT_s}{2\pi M_i}} \qquad (8)$$

and

$$J_b = \beta \sum_i \alpha_{c,i} \rho_{e,i} \sqrt{\frac{RT_e}{2\pi M_i}} \left[e^{-m_i^2} - \sqrt{\pi} m_i \operatorname{erfc}(m_i) \right] \qquad (9)$$

The variable m_i is a dimensionless gas velocity for species i and is defined as

$$m_i = u \sqrt{\frac{M_i}{2RT_e}} = u \sqrt{\frac{M_i}{2RT_e}} \qquad (10)$$

The parameters $\alpha_{v,i}$ and $\alpha_{c,i}$ are the vaporization and condensation coefficients for the individual vaporizing species. These are usually empirically determined and account for any non-

ideal behavior between the actual flux and the ideal flux calculated with $\alpha_{v,i}$ and $\alpha_{c,i}$ set to unity.

The gas fluxes leaving the e and g states can be calculated in the same way as for flux J_s and J_b which give

$$J = \sum_i \rho_{e,i} u_i = \rho_e u = \dot{m} \tag{11}$$

$$J_g = \rho_g u_g = \dot{m}_g \tag{12}$$

and are identical to the intuitive results obtained from continuum flow theory. Finally, utilizing Eq. 5 we obtain the conservation of mass relationship by combining all of the expressions for the four mass fluxes

$$\rho_e u = \dot{m}_g + \sum_i \left\{ \alpha_{v,i} \rho_{s,i} \sqrt{\frac{RT_5}{2\pi M_i}} + \beta \alpha_{c,i} \rho_{e,i} \sqrt{\frac{RT_e}{2\pi M_i}} [\sqrt{\pi} m_i \operatorname{erfc}(m_i) - e^{-m_i^2}] \right\} \tag{13}$$

In a simplified form this is

$$\dot{m}_c = \sum_i \left\{ \alpha_{v,i} \rho_{s,i} \sqrt{\frac{RT_s}{2\pi M_i}} + \beta \alpha_{c,i} \rho_{e,i} \sqrt{\frac{RT_e}{2\pi M_i}} [\sqrt{\pi} m_i \operatorname{erfc}(m_i) - e^{-m_i^2}] \right\} \tag{14}$$

where $\dot{m}_c$ is the net surface vaporization flux.

Conservation of momentum can be satisfied by applying an equivalent procedure for the momentum fluxes

$$P = P_s + P_g - P_b \tag{15}$$

the momentum fluxes can be determined from the second moment of the velocity distributions defined by

$$P = \sum_i \int \xi_i^2 f_i \, dV_i \tag{16}$$

Applying the distribution functions to Eqs. (15) and (16) gives the conservation of momentum relationship

$$\rho_e \left(u^2 + \frac{RT_e}{M_e} \right) = \sum_i \alpha_{v,i} \rho_{s,i} \frac{1}{2} \frac{RT_s}{M_i} + \frac{\dot{m}_g}{\dot{m}} \rho_g \frac{RT_s}{M_g} + \rho_g u_g^2 + \beta \sum_i (2 - \alpha_{c,i}) \rho_{e,i} \frac{RT_e}{M_i} \times \left[\left(m_i^2 + \frac{1}{2} \right) \operatorname{erfc}(m_i) - \frac{m_i}{\sqrt{\pi}} e^{-m_i^2} \right] \tag{17}$$

where

$$\dot{m} = \dot{m}_c + \dot{m}_g \tag{18}$$

Finally, conservation of energy must be considered. For a gas of arbitrary composition, energy is transported via two distinct mechanisms. First, the energy of motion, or the translational energy, contributes to the energy flux. Second, for any nonmonotomic or nonideal monotomic gas, energy is transferred via internal energy modes, i.e., vibration, rotation, etc. The total energy is, therefore, the sum of the two parts

$$e_{\text{tot}} = e_{\text{tr}} + e_{\text{int}} \tag{19}$$

Conservation of total energy requires

$$e_{\text{tot},e} = e_{\text{tot},s} + e_{\text{tot},g} - e_{\text{tot},b} \tag{20}$$

or

$$e_{\text{tr}} + e_{\text{int}} = e_{\text{tr},s} + e_{\text{int},s} + e_{\text{tr},g} + e_{\text{int},g} - e_{\text{tr},b} - e_{\text{int},b} \tag{21}$$

The translational energy can be calculated from the third moment of the velocity by

$$e_{\text{tr}} = \frac{1}{2} \sum_i \int (\xi_i^2 + \eta_i^2 + \zeta_i^2) \xi_i f_i \, dV_i \tag{22}$$

and energy associated with internal degrees of freedom can be obtained from the following general definition:

$$e_{\text{int}} = \left(h = \frac{5}{2} \frac{RT}{M} \right) J \tag{23}$$

Therefore, conservation of energy requires

$$\rho_e u \left(h_e + \frac{1}{2} u^2 \right) = \dot{m}_g \left(h_g + \frac{1}{2} u_g^2 \right) + \sum_i \alpha_{v,i} \rho_{s,i} \sqrt{\frac{RT_s}{2\pi M_i}} \left[h_{s,i} - \frac{1}{2} \frac{RT_s}{M_i} \right] + \beta \sum_i \left\{ \alpha_{c,i} \rho_{e,i} \sqrt{\frac{RT_e}{2\pi M_i}} [(\sqrt{\pi} m_i \operatorname{erfc}(m_i) - e^{-m_i^2}) h_{e,i} + \frac{RT_3}{M_i} \left(m_i^3 \sqrt{\pi} \operatorname{erfc}(m_i) - \left(m_i^2 - \frac{1}{2} \right) e^{-m_i^2} \right)] \right\} \tag{24}$$

In the above conservation equations (14), (17), and (24), there are 14 unknowns: ρ_e, T_e, M_e, h_e, ρ_s, T_s, M_s, h_s, ρ_g, u_g, M_g, h_g, β, and u or m_i if $\dot{m}_c$ and $\dot{m}_g$ are specified. Additional relationships are needed to close the set of equations. Recall that the initial assumptions regarding the velocity distributions implied equilibrium between the solid and the molecules leaving the surface via the flux J_s. Therefore, the following relations are applicable:

$$\rho_s = \rho_s(T_s) \tag{25}$$

$$M_s = M_s(T_s) \tag{26}$$

and

$$h_s = h_s(T_s) \tag{27}$$

which are based on a unique vapor pressure or vapor density equilibrium relationship with temperature at a solid-vapor boundary. At the e and g state, we assume that the gas is in a state of thermochemical equilibrium and, therefore,

$$M_e = M_e(T_e, \rho_e) \tag{28}$$

$$h_e = h_e(T_e, \rho_e) \tag{29}$$

$$M_g = M_g(T_g, \rho_g) \tag{30}$$

and

$$h_g = h_g(T_g, \rho_g) \tag{31}$$

apply. The additional assumption

$$p_g = p_e \tag{32}$$

also is used so that

$$\rho_g = \rho_g(T_s, p_e, M_g) \tag{33}$$

If needed, the pressures can be computed from the ideal gas law, which relates the pressure to the density, temperature, and molecular weight.

The above thermodynamic relationships are expressed numerically using a version of the Aerotherm Chemical Equilibrium (ACE) Code.[8] The ACE Code computes the ideal thermodynamic equilibrium between an arbitrary number of gas and surface species, given the elemental composition of the gas and basic thermodynamic properties of each species. Ideal gas heat capacities are correlated as polynomial functions of temperature and then integrated analytically to obtain enthalpies and entropies of formation. These are then used to form a set of simultaneous equations expressing the equilibrium relationship between the independent chemical reactions of each species. Using a multidimensional Newton-Raphson iteration scheme, species concentrations are obtained as functions of temperature and pressure. From the species concentrations, the bulk gas properties of enthalpy, molecular weight, and density can be computed.

Before the set of model equations presented above can be solved, a restriction upon the bulk flow at the edge of the Knudsen Layer must be imposed. First, consider the case where the external pressure is low. If the irradiance level of the incident radiation is maintained for a longer time than the characteristic relaxation time of molecules across the Knudsen Layer, then the flow of gases from the surface will appear quasisteady. Furthermore, if this irradiation is sufficiently high, the flow will be in the form of a jet directed away from the surface. Based on discussions in earlier sections, the bulk gas velocity will be equal to the speed of sound at the equilibrium, or e state, location. Since the location of the e states is very near the surface, all of the flow is assumed to be directed normally outward from the surface at this location. Therefore, the condition requiring unity Mach number at e is

$$\frac{\dot{m}}{\rho_e}\sqrt{\frac{M_e}{\gamma_e RT_e}} = 1 \tag{34}$$

Now suppose that the irradiance level is high, but not sufficient to produce a sonic flow at the edge of the Knudsen Layer. Then, the flow will resemble a subsonic jet. Under these conditions, the flow geometry cannot accommodate significant radial pressure variations, and the external pressure imposes itself upon the flow. The condition

$$p_e = p_{\text{ext}} \tag{35}$$

is then applicable.

The final model consists of the 16 equations (10–12), (14), (17), (24), (25–33), and (34) or (35). These equations contain 16 unknown if $\dot{m}_c$ and $\dot{m}_g$ are specified. This system of equations is reduced to a set of four equations with four unknowns and is solved numerically using a modified, multidimensional Newton-Raphson iteration procedure to predict surface temperature given the mass loss rate.

Relation to Surface Energy Balance

To relate the mass loss rate and surface temperature to the irradiation rate, it is necessary to introduce the surface energy equation into the solution scheme. The energy equation may take several forms, depending on the assumed conditions for the spatial energy flux distribution, the geometry of the material, or the time-varying history of the heating rate. For simplicity, consider the case of the application of a constant irradiance to the surface of sufficient magnitude to attain quasisteady ablation conditions. At long times, i.e., after the initial heat-up transients, steady-state conditions prevail. Considering the energy fluxes into and out of the control volume centered around the ablating surface, as shown in Fig. 3, conservation of energy requires

$$\alpha I_0 = F\sigma\epsilon T_s^4 + \dot{m}[h_e + (1/2)u^2] - \dot{m}h_\infty \tag{36}$$

The variable T_s is the surface temperature, and $\dot{m}$ represents the total mass flux out of the control volume. The incident irradiation to the surface is denoted by I_0, and the kinetic energy of the gas leaving the Knudsen Layer is $1/2u^2$. The parameters α, ϵ, and F denote the surface absorptivity, emissivity, and view factor, respectively. Here we have evaluated the enthalpy of the gas mixture h_e at the equilibrium, or e state. The base state enthalpy h_∞ is evaluated at T_∞ assuming isothermal conditions far away from the material surface. Reradiation from the surface is assumed to take place at the surface temperature into a low-temperature sink such that the net flux is approximated by the black body radiation function at the surface temperature.

In the steady-state energy equation given by Eq. (36), one is usually interested in determining the mass loss rate and associated temperature given the material properties and the surface energy input. The mass loss vs temperature curves for a specified external pressure can be obtained using the procedure described above. Then, these results can be used to iterate for the mass loss and associated surface temperature using a separate, solution technique.

If steady heating conditions are not achieved, or if the material geometry is irregular and not one-dimensional, the in-depth energy flow must be treated by a transient multidimensional heat equation. In these cases, the mass flux and surface temperature relationship are not spatially uniform and time-independent, but may vary with time and position. In particular, a specially modified version of a transient one-dimensional conduction code CMA[9] is used. This code solves the unsteady heat conduction equation

$$\rho C_p\left(\frac{\partial T}{\partial \theta}\right)_x = \frac{\partial}{\partial x}\left(k\frac{\partial T}{\partial x}\right)_\theta + (h_g - \bar{h})\frac{\partial \rho}{\partial \theta}\Big)_y + \dot{s}\rho C_p\frac{\partial T}{\partial x}\Big)_\theta + \dot{m}_g\frac{\partial h_g}{\partial x}\Big)_\theta \tag{37}$$

in a coordinate system tied to the receding surface. The material density is written in terms of three components

$$\rho = \Gamma(\rho_A + \rho_B) + (1-\Gamma)\rho_C \tag{38}$$

where each of the three components can decompose according to the Arrhenius relation

$$\left(\frac{\partial p_i}{\partial \theta}\right)_y = -B_i e^{-E_{ai}/RT}\rho_{oi}\left(\frac{\rho_i - \rho_{ri}}{\rho_{oi}}\right)^\psi \tag{39}$$

The boundary condition on the moving ablating surface takes the form

$$\alpha I_0 = F\sigma\epsilon T_s^4 + \dot{m}\left(h_e + \frac{1}{2}u^2\right) - \dot{m}_c h_c - \dot{m}_g h_g - q_{\text{cond}} \tag{40}$$

where h_c is the enthalpy of the solid at the surface temperature T_s, and q_{cond} is the heat loss in the solid away from the surface. Information that must be provided as inputs to this code includes the solid material properties of heat capacity, density and thermal conductivity, the enthalpy of the pyrolysis gas as a function of temperature and pressure, and the

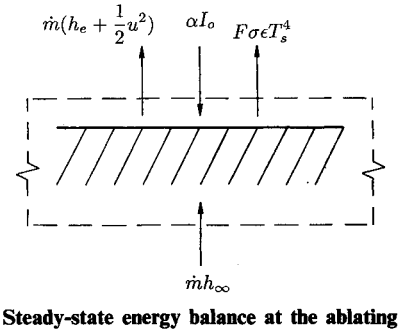

Fig. 3 Steady-state energy balance at the ablating surface.

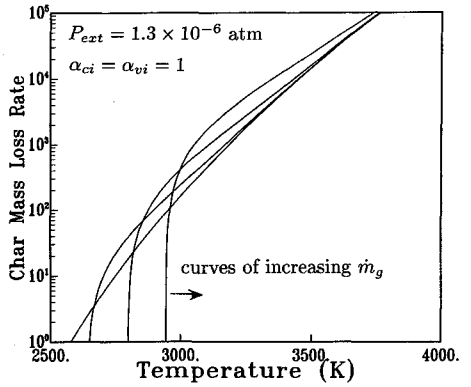

Fig. 4 Char mass loss rate vs surface temperature for carbon phenolic.

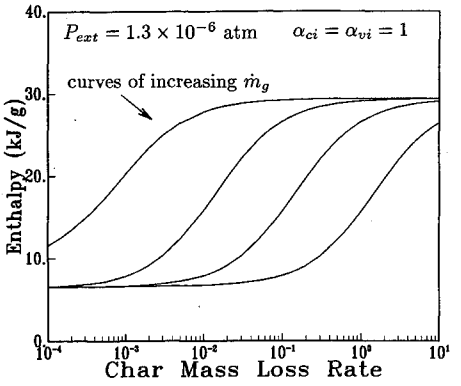

Fig. 5 Calculated *e* state enthalpy as a function of char mass loss rate for carbon phenolic.

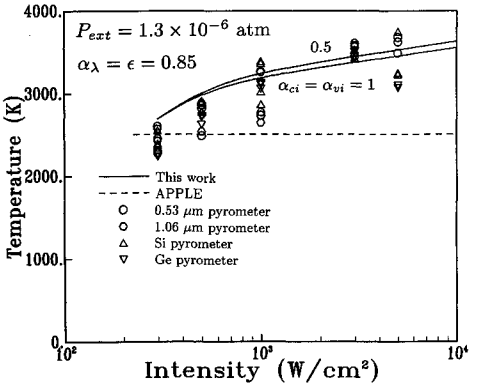

Fig. 6 Steady-state surface temperature vs incident irradiance for carbon phenolic.

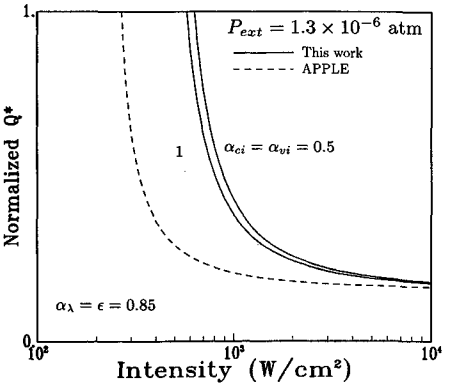

Fig. 7 Steady-state Q^* vs incident irradiance for carbon phenolic.

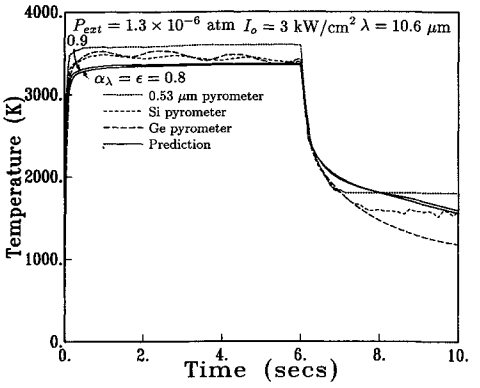

Fig. 8 Predicted and experimental surface temperature vs time for carbon phenolic.

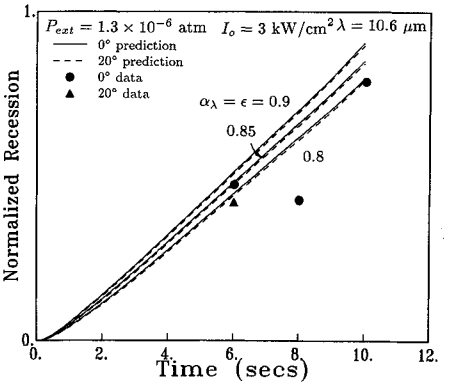

Fig. 9 Predicted vs measured posttest recession for carbon phenolic.

mass loss vs temperature relationship in the form of tabular entries.

Results

Results of the model are shown in Figs. 4-9 for ablation of carbon phenolic into a low-pressure environment. In some cases the results are normalized to some arbitrary value as required by security regulations pertaining to this work. In all predictions, the following gas-phase species were assumed to be in equilibrium: C, C_2, C_3, C_4, C_5, C_6, C_7, CH, CH_4, CO, CO_2, C_2H_2, C_6H_6, H_2, H_2O, N, N_2, O, OH, and O_2. The surface species for all *s* state calculations were taken to be pure carbon. Thermodynamic data for the single-element carbon species were obtained from Lee and Sandborn[10] and Lieder, Krikorian and Young,[11] whereas data for the other species were taken from Stull and Prophet.[12]

Figure 4 illustrates the predicted char mass loss rate vs surface temperature with pyrolysis mass loss rate as a parameter obtained from the new model. The important trend to observe is the continually rising surface temperature vs char mass loss rate. Pure thermodynamic equilibrium would predict a constant surface temperature independent of mass loss for fixed pyrolysis mass loss rate. Figure 5 illustrates the computed *e* state enthalpy as a function of the char mass loss rate. The same assumptions used in generating Fig. 4 are also used here. The backscattering parameter β, which takes on a unique value as a consequence of the solution, varies with both the char and pyrolysis mass loss rate, but has not been shown.

In Fig. 6, the mass loss vs temperature results of the model have been used in conjunction with the steady-state energy balance routine to predict the surface temperature vs incident irradiance for carbon phenolic. Two curves are shown using different values of condensation and vaporization coefficients. The intent of the two curves is to demonstrate that the sensitivity of the predicted temperatures to the surface coefficients is not large, and that even a large uncertainty in

condensation of vaporization coefficients does not lead to an appreciable change in surface temperature. Results from the APPLE model are also shown subject to the incorrect assumption of a surface pressure equal to the bulk, freestream pressure. Surface pyrometer data from two narrow-band 0.53 and 1.06 μm and two broad-band gemanium and silicon pyrometers are shown as discrete points. These data were obtained from recent experiments with a 10.6 μm CW CO_2 laser and represent the long-time, quasisteady temperature. Note that all pyrometer data have been corrected for a surface emissivity of 0.9. The original APPLE model does not consider the new effects developed in this work and does not agree well with the data, especially at high intensities. The new model results include the explicit effects of the Knudsen Layer on the vaporization processes. Predictions of the new model show better agreement with available pyrometer data than the older model.

Figure 7 presents results of recession (as expressed as Q^*_{ss})‡ plotted on an arbitrary scale for the two models. Like the surface temperature predictions, Q^* values are significantly different between the old and the new models, but are still relatively insensitive to the effect varying condensation or vaporization coefficients.

Finally, in Figs. 8 and 9, the results of transient predictions for the ablation of 20-deg shingle-angle carbon phenolic§ at 3.0 k/W/cm^2 are presented. Figure 8 illustrates the temperature time history of a 6-s irradiation for two values of surface absorptivity and emissivity. Again, the results of the model are presented along with measured surface temperatures using several wavelength pyrometers. Although the model slightly underpredicts the measured temperature, the agreement is nonetheless quite good. Ripples in the measured temperature time curve can be attributed to burnthrough of the distinct material plies. The surface temperature momentarily increases as the laser burns through the carbon-rich reinforcement plies and decreases in the resin-rich areas between plies.

The time-dependent recession history of a similar irradiation is presented in Fig. 9 along with some experimental, posttest recessions for flat-layup and single-angle carbon phenolic obtained under the same test conditions. Three curves corresponding to different optical surface properties are presented, illustrating the sensitivity of predicted recession to absorptivity and emissivity. For three of the four data points, the predictions for an emissivity and absorptivity of 0.8–0.85 yield very good agreement.

Conclusions

An extension to the APPLE thermal-ablation code allowing accurate calculation of high rates of ablation for generic hardening materials into a low-pressure atmosphere has been performed. This model retains the generality originally present in the APPLE code and explicitly considers the coupled effects of fluid flow, surface thermochemistry, and in-depth heat conduction. The model uses a nonequilibrium Knudsen Layer formulation that has a well defined, physical interpretation. Parameters used in the model consist of thermodynamic gas-phase properties for the vaporization species and thermal transport properties for the bulk solid. The model is valid for arbitrary hardening materials, provided thermal transport and bulk properties are available.

Predictions with the new model show good correlation with experimental data for the laser irradiation of carbon phenolic. The model explains the rise in temperature with incident irradiance levels and vaporization rates observed in experiments. Pure thermochemical ablation predicts a suface temperature independent of mass loss rate and cannot explain this trend in surface temperature. Posttest recession measurements from irradiated coupons show good agreement with model predictions.

Although this paper has emphasized heating from high-energy lasers, this model finds use in other applications such as radiating shock layers, where radiative heating is the primary thermal transport mode.

Acknowledgment

This work was sponsored by the Air Force Wright Aeronautical Laboratories, Materials Laboratory, Wright-Patterson Air Force Base, Ohio under Contract No. F33615-83-C-5074.

References

[1]Kendall, R. M., Rindal, R. A., and Bartlett, E. P., "A Multicomponent Boundary Layer Chemically Coupled to an Ablating Surface," *AIAA Journal*, Vol. 5, June 1967, pp. 1063–1071.

[2]Kendall, R. M., "An Analysis of the Coupled Chemically Reacting Boundary Layer and Charring Ablator, Part V: A General Approach to the Thermochemical Solution of Mixed Equilibrium-Nonequilibrium, Homogeneous or Heterogeneous Systems," NASA CR-1064, June 1968.

[3]Tong, H., et al., "Radiant Heating of Aerospace Materials, Part II: Laser Effects Prediction Procedure Code," AFML-TR-73-190, Part II, June 1975.

[4]Anisimov, S. I., "Vaporization of Metal Absorbing Laser Irradiation," *Soviet Physics JETP*, Vol. 27, 1968, pp. 182–183.

[5]Knight, C. J., "Theoretical Modeling of Rapid Surface Vaporization with Back Pressure," *AIAA Journal*, Vol. 17, May 1979, pp. 519–523.

[6]Baker, R. L., *Carbon Nonequilibrium Phase Change*, Aerospace Corp. Rept. SD-TR-81-89, 1981.

[7]Risch, T. and Kelly, T. H., "A Model for Radiation Driven Ablation of Carbon Under Low Pressures," *SAE Transactions*, Vol. 5, 1985, Article 851396, pp. 477–485.

[8]*User's Manual Aerotherm Chemical Equilibrium Computer Program*, Acurex, Rept. UM-81-11/ATD, Aug. 1981.

[9]*User's Manual Aerotherm Charring Material Thermal Response and Ablation Program, Version 3*, Rept. AFRPL-TR-70-92, April 1970.

[10]Lee, E. L. and Sandborn, R. H., "Extended and Improved Thermal Functions for the Gaseous Carbon Species C_1–C_7 from 298 to 10000 K," *High Temperature Science*, Vol. 5, 1973, pp. 438–453.

[11]Lieder, H. R., Krikorian, O. H., and Young, D. A., "Thermodynamic Properties of Carbon Up to the Critical Point," *Carbon*, Vol. 11, 1973, pp. 555–563.

[12]Stull, D. R. and Prophet, H., "JANAF Thermochemical Tables," 2nd ed. U. S. Dept. of Commerce, National Bureau of Standards, NSRDS-NBS 37, 1971.

‡Q^*_{ss} is defined as $I/\rho\dot{s}$ where I is the incident irradiance, ρ is the material density, and $\dot{s}$ is the steady-state recession rate.

§Shingle angle and flat layup denote the orientation of the composite plies relative to the material surface. In flat layups, the reinforcement plies are oriented parallel to the surface, whereas in shingle-angle layups, the plies run at a slight angle.